International Journal of
INTELLIGENT SYSTEMS AND APPLICATIONS IN ENGINEERING
ISSN:2147-6799 www.ijisae.org Original Research Paper

# Breast Cancer Detection Using Image Denoising and UNet Segmentation for Mammography Images

**[1]M. Subha, [2]P. Srimanchari**

**Submitted**: 03/02/2024 **Revised**: 11/03/2024 **Accepted**: 17/03/2024

**Abstract:** Breast cancer remains a significant global health concern, necessitating the development of effective risk assessment for detection and prevention. It is a worldwide health issue that requires enhanced early detection methods. In this paper represents breast cancer detection technique using advanced learning techniques. Initially the dataset has collected form benchmark datasets as Mammography with Benign Malignant Masses with three categories like MIAS, Inbreast and DDSM. The Dataset has trained using VGG19 with Modified Densenet. The Image Denoising has used Non local mean with Wavelet (NLW) Algorithm. NLW denoising minimizes noise and preserves features, guaranteeing high-quality images for analysis. Image segmentation has done using WaterUNet model. WaterUNet model is correctly identifies malignant spots in mammography images. Finally, the classification has done with VGG19 algorithm with 99% accuracy. Experimental results show that the proposed technique outperforms with existing approaches like accuracy, precision, recall and f-measure.

**Keywords:** *Breast Cancer, DenseNet, Mammography, NLW, VGG19, WaterUNet*

## I. Introduction

When it comes to illnesses that mostly impact women, breast cancer is one of the most prevalent worldwide. This cancerous growth begins in the milk ducts or lobules of the breast [1]. Early identification and accurate diagnosis are crucial for effective treatment and improved survival rates [2] because to the devastating effects of breast cancer on individuals, families, and communities. Advances in medical imaging and machine learning approaches have transformed breast cancer screening in recent years [3]. Early identification is critical to enhancing the likelihood of effective therapy and long-term survival. Mammography, a low-dose X-ray imaging technology, has long been used to screen for breast cancer [4]. However, properly reading mammograms can be difficult, and false positives or negatives can occur [5]. To address these issues, researchers and healthcare professionals have been investigating novel approaches and technologies to improve the accuracy and efficiency of breast cancer diagnosis [6]. This has resulted in the development of complex algorithms, neural networks, and image processing approaches that harness the power of artificial intelligence to accurately evaluate mammography images [7].

[1]*Ph.D Research Scholar, PG and Research department of Computer Science, Erode Arts and Science College(Autonomous), Erode-09. Tamil Nadu, India.*
*subha.gmanoharan@gmail.com*
[2]*Research Guide and Assistant Professor of Computer Science, PG and Research department of Computer Science, Erode Arts and Science College (Autonomous), Erode-09, Tamil Nadu, India*

Breast cancer is one of the most common and deadly illnesses in the world, making early identification and correct diagnosis critical for successful treatment and improved patient outcomes [8]. The gold standard for breast cancer screening is mammography, an X-ray imaging procedure. However, mammography interpretation can be difficult due to the complex and nuanced nature of breast tissue structures, which are frequently masked by noise and aberrations [9]. To overcome these issues, sophisticated computational approaches, notably image denoising and segmentation, have emerged as critical components in improving the accuracy of breast cancer diagnosis from mammography images [10].

Deep learning-based approaches have shown exceptional effectiveness in a variety of medical image analysis applications in recent years [11]. CNNs, such as VGG19 and DenseNet, have demonstrated greater skills in feature extraction from complicated images [12]. Furthermore, semantic segmentation algorithms such as U-Net have transformed the field by providing pixel-level classification, making them ideal candidates for defining malignant spots in mammograms [13]. This study investigates a complex strategy that combines the strength of these techniques: a hybrid neural network incorporating VGG19 and modified DenseNet that is optimized using an enhanced Stochastic Gradient Descent (SGD) algorithm for developing a robust breast cancer detection model [14]. Furthermore, the quality of mammography images has a considerable impact on cancer diagnosis accuracy [15]. The presence of noise and distortions in these photos might lead to

misunderstanding and false positives. Advanced denoising methods are required to alleviate this [16]. In this paper, we use a cutting-edge denoising approach based on the Non-Local Means with Wavelet (NLW) transformation [17]. NLW denoising successfully maintains critical picture information while reducing noise, resulting in high-quality mammograms for later analysis [18-20].

The primary contributions and objectives of this manuscript can be summarized as follows.

- Image dataset training using hybrid neural network VGG19 with modified DenseNet optimization using improved SGD optimization
- Image Segmentation Using Waterunet Architecture

The rest of this paper will look like this. Several methods for predicting breast cancer are discussed by several writers in Section 2. In Section 3, we can see the suggested model. In Section 4, we provide a brief overview of the study's findings. The conclusion and recommendations for further research are presented in Section 5.

### 1.1 Motivation of the paper

This research aims to improve breast cancer detection to solve the global health issue. A global concern, breast cancer requires effective risk assessment for identification and prevention. This work uses a broad benchmark dataset and sophisticated learning methods. Training with VGG19 and Modified Densenet ensures robust analysis. Denoising using Non local mean with Wavelet (NLW) Algorithm preserves key characteristics for proper interpretation, improving picture quality. WaterUNet, developed to detect cancerous areas in mammograms, segments images. Validated using VGG19, the suggested method is 99% accurate. This method outperforms others in accuracy, precision, recall, and f-measure, suggesting it might change breast cancer diagnosis.

## 2. Background Study

A.Intasam et al. [1] authors research addresses the shortcomings of existing breast cancer diagnostic and treatment strategies by analyzing a model for lesion detection in mammography images. Patients were more likely to obtain correct diagnoses and effective treatments according to the findings of this study, which can also reduce the number of tests that aren't essential.

D. Fajri Riesaputri et al. [5] proposes utilizing the probabilistic neural network (PNN) method as a classifier to distinguish between normal, benign, and malignant breast cancer images. Several preparation processes, including scaling to compute computations and equalize size, converting to grayscale to provide Gray-Level Co-Occurrence Matrix (GLCM) feature extraction, and employing a median filter to eliminate noise, allowed for effective classification on a tiny dataset. Complete success in labeling the test data.

G. Latif et al. [8] The process of identifying the kind of breast cancer and making a diagnosis at an early stage was crucial. Early detection of cancer, especially breast cancer, allows medical professionals to consider treatment options that might save the lives of their patients. To despeckle breast ultrasound images and classify breast cancers as benign or malignant, respectively, two convolutional neural network (CNN) models were proposed in this study. The Mendeley Breast Ultrasound dataset was used to evaluate the suggested models. CNN despeckler and the CNN classifier have been shown to attain a classification accuracy of 88.00%, which was greater than the accuracies of other systems in the literature.

K. P. Adila and K. Sheeba [10] Classification of mammography images now makes use of a feature fusion approach that was just recently established. The highest rate of success was 64.70 percent. The suggested approach makes advantage of the AlexNet CNN architecture. Classification outcomes need to be 100% exact, as the biological situation has direct bearing on the patient's life. Despite the small size of the mammography dataset, the suggested study improves upon the current model. Data augmentation in the MIAS dataset using a variational auto encoder was being studied for its efficacy.

M. U. Hoque et al. [12] Manual breast cancer tissue identification takes more time and has a variable success rate depending on the expertise of the examiner. A simplified, faster, and more accurate automated method was suggested in this research. The study's goal was to find a way to improve upon the accuracy of pathologists in identifying breast cancer tissues. The test findings and accuracy rate have been recognized by pathology laboratory specialists.

N. F. Razali et al. [15] Models have been trained on AlexNet and InceptionV3 pre-trained networks, with input images from the INbreast and computer-based information systems- Detention, Demurrage, Storage, and Monitoring (CBIS-DDSM) datasets of mammography used to assess performance. The photographs were preprocessed with both augmented and unaugmented settings. As a result of these authors studies, the author conclude that incorporating high-level properties into InceptionV3's deeper layers can improve the system's performance when diagnosing a variety of

breast disorders. The key to effectively applying pre-trained CNN to medical image collections was to modify the training options and fine-tune the hyperparameter in the proposed models. Finally, it was possible to get optimal results by combining the best available pre-trained network with high-quality input photos and suitable picture pre-processing techniques, such as enhancement and augmentation.

P. K. Samanta et al. [17] Here, the author examine the CNN model's performance in identifying breast cancer subtypes from ultrasound images. Applying Transfer Learning to the process of categorizing photos has also produced promising results. The BCI-Net model employs the Mish activation function to boost performance and training dynamics. The model can be trained with more activation functions in the future to improve its overall performance. The proposed BCI-Net achieves a consistent 98.70% accuracy across all simulations on the BUSI dataset. Furthermore, this unique deep CNN can be used for a wide variety of medical imaging applications, not just breast cancer diagnosis.

T. Gayathri et al. [20] The Mayfly algorithm (MFA) was used to improve CNN's learning speed in this research. Experiments analyzing segmentation and classification performance were conducted on two datasets, MIAS and CBIS-DDSM datasets, with respect to a number of distinct factors. According to the obtained data, the suggested MFA-CNN outperformed the CBIS-DDSM dataset on the MIAS dataset across all evaluated metrics. New meta-heuristics algorithms and deep learning approaches need to be developed to increase the classification accuracy of the current study.

Y. Feng et al. [22] The absorption coefficient, average refractive index, scattering coefficient, and anisotropy factor are required by the Monte Carlo model since they are based on the physical characteristics of photons in biological tissues. Having established that the breast consists of six layers (skin, fat, glandmuscle, fat, and skin), we moved on to characterize the characteristics of both the simulated cancer tissue and the normal breast tissue. Finally, transmittance curves for both normal and cancerous breast tissue were generated using the Monte Carlo model. Computational simulations were used to confirm the Monte Carlo model's correctness.

Z. KHOMSI et al [24] The author used COMSOL simulations to demonstrate that breast surface temperature gradients might be studied to identify cancer. The author has built a phantom using a carefully selected set of organic materials to test the efficacy of the integrated system for detecting breast cancer in the lab. Submerged temperature-controlled resistors were used to represent tumors.

### 2.1 Problem definition

The problem addressed in this paper revolves around the pressing issue of breast cancer, a significant global health concern. Early detection is crucial for effective treatment and prevention, necessitating the development of advanced techniques for accurate risk assessment. Despite efforts, current methods often fall short in terms of accuracy and efficiency. This research aims to tackle this problem by proposing a comprehensive breast cancer detection technique that combines state-of-the-art technologies, including advanced machine learning algorithms and innovative image processing methods. The study specifically focuses on enhancing the quality of mammography images, accurately identifying malignant spots, and achieving a high level of precision and accuracy in the classification process.

## 3. Materials and Methods

The proposed model for tackling the challenges in breast cancer prediction is described in this article. Image datasets were trained using a hybrid neural network VGG19 and modified densenet optimization with improved SGD optimization. Denoising images using Wavelet and Non-Local Means. Finally, WaterUNet Architecture is employed in the prediction of breast cancer. The breast cancer detection using image denoising and UNet segmentation for mammography images model flowchart has represented at figure 1

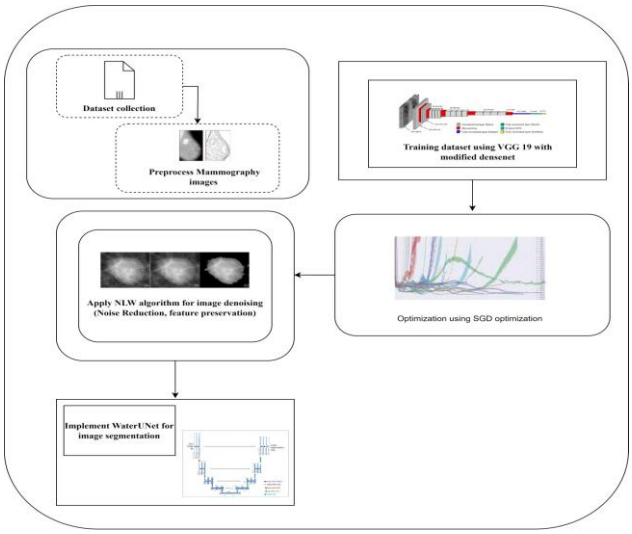


Figure 1: Proposed work flow

### 3.1 Dataset Gathering

The dataset has collected from https://data.mendeley.com/datasets/ywsbh3ndr8/2 with 786MB size. The collection includes both benign and malignant tumors seen on mammograms. The 106 INbreast images, 53 MIAS photos, and 2188 DDSM images used here were all obtained from other datasets. We next perform contrast-limited adaptive histogram equalization and data augmentation as part of our first picture processing. The augmented data sets include a total of 7632 images for Inbreast, 3816 for MIAS, and 13128 for DDSM. Additionally, we combine INbreast, MIAS, and DDSM. Every picture was shrunk down to 227x227 pixels.

### 3.1 Image dataset training using VGG19 with Modified DenseNet

#### 3.1.1 VGG19

There are five 2*2 convolution layers and one 2*2 maximum pooling layer in a VGG19 network, each with a step size of 2 totally 25 layers; Each of the first two layers contains 4096 channels, while the third has 1000 channels, which stands for 1000 different label categories D. Kusumawati et al. (2022). Following each discrete layer, a relu nonlinear activation function is utilized; the local response normalization (LRN) suggested in alexnet is found to boost performance minimally at best and cause severe memory loss in practice. The softmax layer serves as the last layer. The protein VGG19 is shown here on a grand scale.

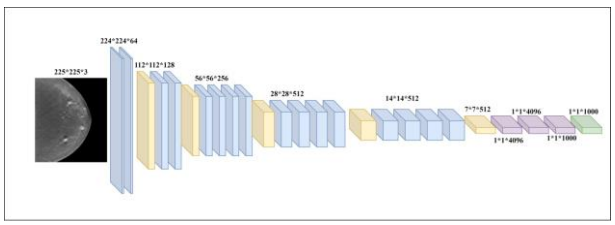

Figure 2: Network structure diagram of VGG19

VGG19 was designed to be easily expanded. Each block consists of many convolution layers or full connection layers, with a uniformly sized convolution kernel of 3. The first sample test showed that VGG19 is divided into 6 distinct parts. Each module makes use of the same convolution layer. The options for each module's network layer are described in the preceding paragraph. The feature map is reduced in size by using a parameter called the maxpool, which is the maximum pool level between modules.

The following is the standard 227*227 input image specification for VGG19. The generated picture has the following dimensions since the number of channels was doubled from 3 to 64 after the first convolution layer and the width and height were cut in half from 224 to 112 in the maximum pooling layer: 112 * 112 * 64. The output of three full connection layers is 1 x 1 1000, or 1000 values, which is similar to the 7 * 7 * 512 output of the last convolution layers. When input into the softmax activation function, these 1000 values are scaled down to the range [0, 1], for a grand total of 1. Probability that a picture corresponds to each category is correctly captured by the resultant 1000 numbers.

#### 3.1.2 Modified DenseNet

The input image, $x_0$, is represented by the function H, while the output of the $i^{th}$ layer, $x_i$, is represented by the function H . Given that the outputs of all preceding levels are sent into the $i^{th}$ layer as input. Here is how the formula looks like D. Deepa et al. (2022):

$$x_i = H([x_0, x_1, x_{i-1}]) \text{ ------ (1)}$$

Where the sum of all preceding layers' outputs is $[x_0, x_1, x_{i-1}]$. The several dense blocks that make up DenseNet are linked together via a transition layer. The feature map size for the first block is h w, the second block's map is h 2 * 2, and the third block's map is h 4 * 4. For each convolution module in DenseNet, the number of feature-maps generated as an output is fixed at k.

There will soon be an excessive amount of input feature-maps as DenseNet is refined. The author solved this issue by inserting an 11 convolution module (as bottleneck layer) prior to the 33 convolution layer. Typically, a 4k configuration is used to generate bottleneck layer(1 1Conv) output feature-maps. Therefore, we use a uniform input size of 4k across all 3x3 Conv layers. The transition layer's feature-map count can be trimmed down to make the model more compact. In a typical configuration, we use a decreased set of feature-maps by a factor of 1.2. DenseNet-BC is the name for this specific kind of DenseNet.

### 3.1.3 VGG19 with modified DenseNet

VGG19's base layers are used to capture low-level features, while DenseNet blocks are included into the model's intermediate layers. The first 13 convolutional layers of VGG19 have not modified, thus it can still recognize common visual patterns. DenseNet blocks are introduced at the 14th layer, allowing each layer to accept inputs from all preceding layers inside the block, hence increasing the model's depth with dense connectivity. With the help of gradient flow and feature reuse, the model can efficiently and accurately recognize complex patterns in photos. VGG19's completely linked layers for high-level feature integration cap off the architecture, resulting in a comprehensive framework that performs very well across a wide range of computer vision applications. DenseNet is a cutting-edge deep learning architecture that has recently garnered traction among scientists. Recent research has shown that convolutional networks benefit greatly from shorter connections between their input and output layers, leading to greater depth, accuracy, and efficiency. Dense Net is an improved variant of Resnet that employs element-wise addition inside its concealed layers. The building blocks of a dense net are a dense block and the transition layers, i.e.

**Algorithm 1: VGG19 with Modified DenseNet**

**Input:**

- Mammography images (standardized size, normalization, etc.) represented as x0x0.

**Steps:**

- **Architecture:** VGG19 consists of five 2x2 convolution layers and one 2x2 maximum pooling layer. The first two layers have 4096 channels each, and the third has 1000 channels representing different label categories. ReLU activation functions follow each discrete layer, and a softmax layer serves as the last layer.
- **Input Image Specification:** Standard 227x227 input images are used. The output of the last convolution layers is 1x1x1000, representing the probabilities of the image belonging to each category after softmax activation.
- **DenseNet Structure:** DenseNet incorporates dense blocks where the output of each layer is concatenated with the inputs of all preceding layers inside the block. Transition layers are used to link these dense blocks. The number of feature maps generated by each convolution module is fixed at kk. To handle excessive feature-maps, a bottleneck layer (1x1 convolution) is added before the 3x3 convolution layer.

$$x_i = H([x_0, x_1, x_{i-1}])$$

- **DenseNet-BC:** This variant of DenseNet, named DenseNet-BC, uses a reduced set of feature-maps in transition layers to make the model more compact.

**Output:**

The final output represents the probabilities of the input mammography image belonging to different classes (benign or malignant).

### 3.1.4 Improved Stochastic Gradient Descent optimization

When it comes to training various machine learning models, DNN often use SGD as an optimization technique M. Wang et al. (2020). For the following empirical risk minimization issues, we use SGD:

$$\min_{x \in R^d} F(x) = \frac{1}{N} \sum_{i=1}^{N} f_i(x) \text{ ------- (2)}$$

Parameter values for the model (x) and sample size (N) The loss function, denoted by F(x), might have several shapes depending on the context.

The main idea behind the SGD algorithm is to reduce the value of the objective. The goal function gradient is used to inform an update to the associated parameter values. Here is the revision policy:

$$x^{(t)} = x^{(t-1)} - \mu * G \text{ -------- (3)}$$

Where G is the gradient; Ʉ is the learning rate.

However, SGD is basically a sequential algorithm because of its nature. The model is a direct offspring of its predecessor, as stipulated by the laws governing model updates. Since $x^{(t-1)}$ is required for the update of $x^{(t)}$, the algorithm's parallelism is severely constrained. The parallel stochastic gradient descent algorithm has been the subject of research in recent years. And other suggested parallel algorithms, like Hogwild ASGD, can enable parallelism by lowering the reliance amongst workers to analyze several samples simultaneously. However, all workers' parameter data is necessary for SSGD to function, which results in strong network coupling.

### 3.2 Image denoising using Non-Local Means with Wavelet

To effectively reduce noise without losing picture information, the Non-Local Means with Wavelet method combines wavelet transformation with Non-Local Means filtering S. Zhang and L. Wang (2021). To begin, the noisy image is transformed using wavelets to isolate its frequency components. These altered coefficients are then subjected to Non-Local Means filtering, which highlights correlated regions while simultaneously suppressing background noise. The algorithm's use of the wavelet domain allows for adaptive denoising of images at varying scales, protecting valuable structure and texture along the way. At last, the pristine picture is reconstructed using an inverse transformation of the denoised coefficients. This technique is useful for improving picture quality in many different industries, but it is especially important in areas like medical imaging and remote sensing where noise reduction is necessary for precise interpretation.

By comparing patches with similar backgrounds, generating weights based on similarity, then averaging pixels using those weights, NL means can get better results than just averaging close pixels.

In equation 4, the NL means equation is expressed as

$$f(s) = \frac{\sum_t w(s,t)g(t)}{\sum_t w(s,t)} \text{ ------- (4)}$$

Where $w(s,t)$ denotes the weight between s-patch and t patch. $f(s)$ denotes the estimated intensity in s-pixel. The weights $\sum_t w(s,t)$ can be expressed as

$$w(s,t) = \exp\left[-\frac{1}{h}\sum_k \log\left(\frac{A(s+k)}{A(t+k)} + \frac{A(t+k)}{A(s+k)}\right)\right] \text{ ---------- (5)}$$

In this equation, $\frac{A(s+k)}{A(t+k)}$ represents the amplitudes of individual pixels, g is a filtering parameter, and $\frac{A(t+k)}{A(s+k)}$ is a variable that depends on the whole image.

### 3.3 Image Segmentation Using WaterUNet Architecture

#### 3.3.1 U-Net Segmentation

One of the most well-known segmentation models, UNet, was the first to suggest using an encoder-decoder neural network and skip connections M. Robin et al. (2021). Fig. 3 depicts UNet's network architecture. To encode data into a latent space, the model takes an image as input and processes it with various layers of convolution, max-pooling, and ReLU activation. For the picture segmentation mask, the network employs a transposed convolution operation (deconvolution) to extract information from the latent space. The remaining steps in the encoder function similarly to those described before. Unlike the traditional encoder-decoder architecture, Unet makes use of skip-connections to transmit data from the encoder's high-resolution layers to the decoder, allowing the network to more accurately capture the finer features contained in high-resolution images.

During training, UNet employs the loss function in Eq. (6) in the same way as other neural segmentation models do.

$$l_{Unet} = \sum_{x\in\pi} w(x) \log\left(p_{l(x)}(x)\right) \text{ ------- (6)}$$

Considering that is smaller than Z2 and K is the total number of classes, we get: where: 1,..., K. If we calculate the cross-entropy in binary form, K=2. In addition, the activation in the feature channel, denoted, is used to construct the soft-max: $\sum_{x\in\pi} w(x) \log\left(p_{l(x)}(x)\right)$.

The starting weights have a substantial effect on performance in a network with multiple convolutional layers. For this purpose, network feature maps with starting weights that vary by around a unit were most effective. Using a Gaussian distribution with a standard deviation of 2N is an efficient approach in networks with convolutional and ReLU layers like Unet. Here, N is the number of inputs to a single neuron.

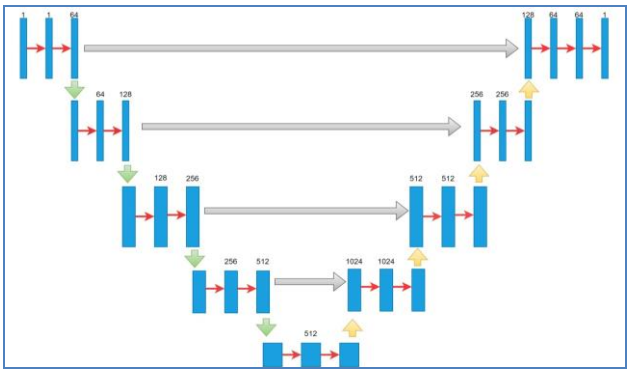

Figure 3: U-Net architecture

### 3.3.2 WaterUNet segmentation

Our approach overcomes the excessive segmentation issue of the conventional watershed transformation by making use of previously acquired information. The usual watershed segmentation approach for the discrete case utilizing topographical distance is briefly discussed here. For a more in-depth analysis, please see the references.

Pixel p in the input image f has a maximum slope $LS(p)$ if compared to its low-altitude neighbors, and this can be written as

$$LS(p) = \max_{q \in N(p) Up} \left( \frac{f(p)-f(q)}{d(p,q)} \right) \text{------- (7)}$$

pixels p and q, and the Euclidean distance between them, $d(p,q)$. The right-hand side of (7) is required to be zero when q = p, therefore even if p is a local minimum, we still have a reduced slope value. Moving from point p to point q is so expensive that

$$cost(p,q) = \begin{cases} LS(P).d(p,q) & if\ f(p) > f(q), \\ LS(q).d(p,q) & if\ f(p) < f(q) \\ \frac{1}{2}[LS(p) + LS(q)].d(p,q) & if\ f(p) = f(q) \end{cases} \text{--------}$$

(8)

The topographical distance between two pixels p and q along the route p = (p0,...,pl) from p0 = p to pl = q is defined as

$$T_f^{\pi}(p,q) = \sum_{i=0}^{l-1} d(p_i,p_{i+1})\, cost(p_i,p_{i+1}) \text{-------- (9)}$$

The shortest path between locations p and q is denoted by the topographic distance T p f p; q>. According to a comparable definition, the catchment basin $CB_{mi}$ of a local minimum mi is the collection of pixels with the shortest topographical distances to mi. Finally, there is a group of pixels known as the watershed that do not belong to any catchment basin. Please take into account that the gradient magnitude picture is often used for the computation of the watershed transformation rather than the gray value image.

UNET's structure consists of a contraction path, or en coder, and an expanding path, or decoder that is symmetric. The encoder is capable of extracting the image's context. The standard max pooling and convolution layers are shown as a stack in the contraction route. As a result, the UNET architecture transforms into a full-blown Fully Convolutional Network (FCN). With just the Convolutional layers and no thick layer, it can handle data of any size.

Our model further develops the underlying structure of UNet. The U-shaped UNet design is the product of an encoder-decoder construction. The same number of decoders as there are encoders comes next. We employ four encoder-decoder modules, similar to the original UNet system.

**Algorithm 1: Water U-Net**

**Input :**

The original grayscale or color image you want to segment.

**Step:**

- **Calculate Maximum Slope$LS(p)$:** For each pixel pp, compute the maximum slope using Equation (7) by comparing its intensity with its low-altitude neighbors and considering the Euclidean distance between them.
- **Compute Cost$cost(p,q)$:** Use Equation (8) to calculate the cost of moving from pixel pp to pixel qq, considering the gradient slopes and Euclidean distances.
- **Compute Topographical Distance $T_f^{\pi}(p,q)$:** Calculate the topographical distance between pixels pp and qq using Equation (9) along the route p=(p0,...,pl)p=(p0,...,pl) considering the distance and cost between consecutive pixels in the route.
- **Identify Catchment Basins (CB(mi)):** For each local minimum point mimi, find the collection of pixels

belonging to its catchment basin by finding pixels with the shortest topographical distances to mimi.

- **UNET Encoding:** Utilize the encoder part of the modified UNet to extract contextual features from the input image.
- **UNET Decoding:** Use the decoder part of the modified UNet to reconstruct the segmented image based on the features extracted by the encoder.

**Output:**

1. **Segmented Image:** The main output is the segmented image, where pixels are grouped into different segments or regions based on the combined approach of watershed transformation and UNet architecture.

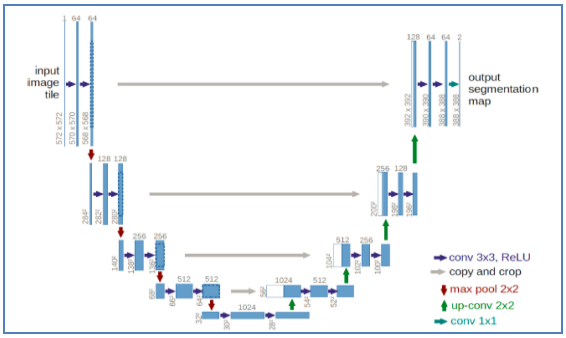


Figure 4: WaterUNet Architecture

The proposed UNET architecture is shown in Figure 4, with the input picture size set at 227*227. However, 128 pixels by 128 pixels by 3 pixels are also used by a number of studies. In order to get the best results, specialists need to examine the photographs from several angles.

### 4. Results and Discussion

In the results and discussion section, the outcomes of the applied breast cancer detection techniques are evaluated and analyzed. This section provides insights into the effectiveness of the proposed methods and discusses how they contribute to the advancement of early detection and diagnosis of breast cancer.

### 4.1 Performance evaluation

Each category was used as a positive sample to determine the overall accuracy, precision, and recall values. Equation (10) can be used to represent the precision as follows:

$$Accuracy = \frac{Numberofsamplescorrectlyclassified}{Numeberofsamplesforallcategories}$$

------ (10)

The precision of a particular category may be interpreted as a prediction of the accuracy of the sample, as shown in Equation (11):

$$Precision_i = \frac{TP_s}{TP_s + FP_s}$$ ------ (11)

The recall of a particular category can be regarded as the amount to which the properly predicted sample of category s covers the sample of category s in the sample set, as shown in Equation (12),

$$Recall_i = \frac{TP_s}{TP_s + FN_s}$$ ------- (12)

F measure is calculated by giving the Equation.

$$F - Measure = 2.\frac{Precison.recall}{Nprecison + recall}$$ ------- (13)

**Table 1: Training and testing accuracy for different datasets**

| | MIAS | | INbreast | | DDSM | |
|---|---|---|---|---|---|---|
| Methods | Training Accuracy | Testing Accuracy | Training Accuracy | Testing Accuracy | Training Accuracy | Testing Accuracy |
| CNN | 87 | 86 | 82 | 81 | 87 | 85 |
| DCNN | 88 | 88 | 83 | 80 | 88 | 86 |
| VGG19 | 89 | 86 | 87 | 86 | 89 | 88 |
| Densenet | 90 | 89 | 88 | 88 | 91 | 90 |
| Modified Densenet | 91 | 89 | 90 | 90 | 91 | 90.2 |
| VGG19 with modified Densenet | 92 | 90.8 | 91 | 90.4 | 92 | 91.5 |

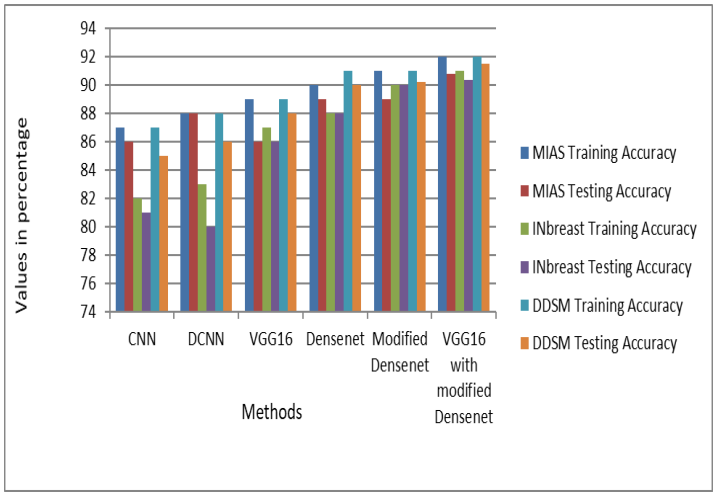


Figure 5: Training and testing accuracy chart

The table 1 and figure 5 shows, the performance of various methods for breast cancer detection using different datasets (MIAS, Inbreast, and DDSM) is evaluated in terms of training and testing accuracy. Traditional Convolutional Neural Networks (CNN) exhibited decent accuracy across all datasets, with a training accuracy ranging from 82% to 87% and testing accuracy between 80% and 86%. The introduction of more complex architectures like Deep Convolutional Neural Networks (DCNN) and established models such as VGG19 and Densenet improved accuracy, with VGG19 achieving a maximum of 89% training and 88% testing accuracy. However, the proposed Modified Densenet method outperformed these models, reaching up to 91% training and 90.2% testing accuracy across the datasets. The integration of VGG19 with Modified Densenet showcased the highest accuracy, achieving 92% training and 90.8% testing accuracy for MIAS, 91% training and 90.4% testing accuracy for Inbreast, and 92% training and 91.5% testing accuracy for DDSM. These results highlight the effectiveness of the hybrid approach, emphasizing the significance of incorporating modified Densenet into existing models for enhanced breast cancer detection accuracy across diverse datasets.

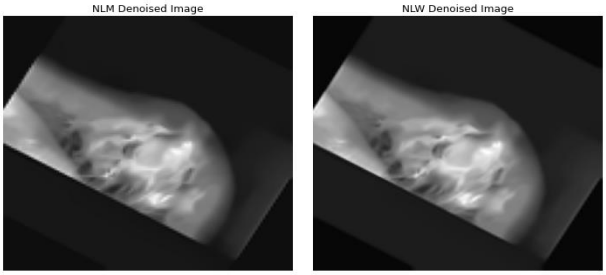


Figure 6: Denoised image

Figure 6 presents denoised images resulting from the application of the proposed denoising technique. These images have undergone a process to reduce noise while preserving critical details and structures.

**Table 2: Image Denoising Evaluation Metrics for NLM and NLW**

| | | NLM | | | NLW | | |
|---|---|---|---|---|---|---|---|
| MIAS Dataset | | PSNR | SSIM | RMSE | PSNR | SSIM | RMSE |
| | Image 1 | 24.4 | 0.73 | 15.2 | 32.4 | 0.92 | 2.04 |
| | Image 2 | 22.1 | 0.75 | 12.8 | 35.6 | 0.91 | 1.41 |
| | Image 3 | 23.8 | 0.88 | 16.1 | 33.4 | 0.93 | 1.56 |
| | Image 4 | 25.7 | 0.71 | 11.6 | 33.2 | 0.93 | 2.45 |
| | Image 5 | 29.3 | 0.63 | 18.4 | 33.8 | 0.92 | 2.01 |
| INbreast | Image 1 | 19.2 | 0.66 | 12.5 | 30.5 | 0.93 | 2.41 |

| | | | | | | | |
|---|---|---|---|---|---|---|---|
| | Image 2 | 18.5 | 0.74 | 12.8 | 29.9 | 0.94 | 2.78 |
| | Image 3 | 22.6 | 0.82 | 14.5 | 31.5 | 0.97 | 2.65 |
| | Image 4 | 29.4 | 0.87 | 19.5 | 37.5 | 0.93 | 3.89 |
| | Image 5 | 28.1 | 0.84 | 11.2 | 32.9 | 0.96 | 3.75 |
| DDSM | Image 1 | 28.7 | 0.79 | 10.5 | 31.9 | 0.91 | 4.81 |
| | Image 2 | 26.9 | 0.88 | 9.8 | 30.4 | 0.90 | 6.45 |
| | Image 3 | 22.1 | 0.89 | 11.1 | 31.8 | 0.96 | 2.51 |
| | Image 4 | 29.7 | 0.82 | 15.4 | 32.9 | 0.97 | 2.09 |
| | Image 5 | 21.3 | 0.76 | 16.8 | 33.8 | 0.98 | 1.89 |

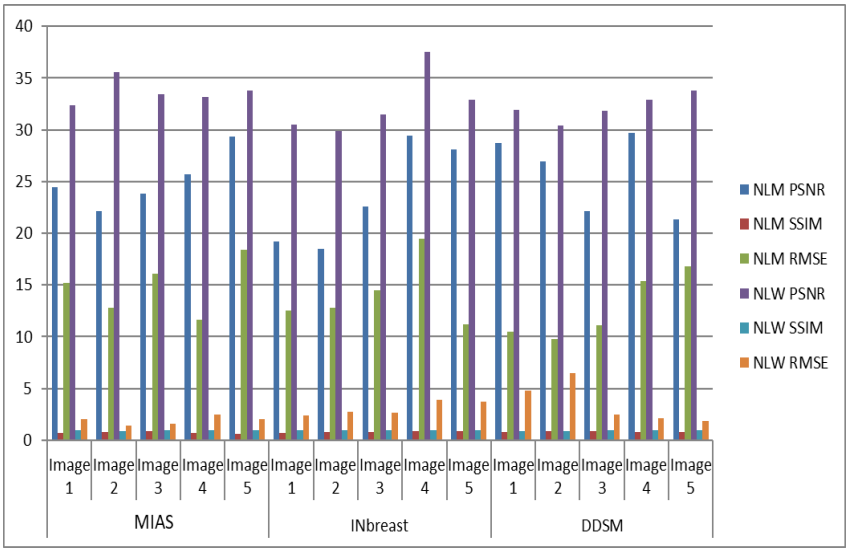


Figure 7: Image Denoising value comparison chart

Across the MIAS dataset, Non local means with Wavelet (NLW) consistently outperforms Non-Local Means (NLM) in image denoising showing in table 2 and figure 7. For example, in Image 1, NLW achieves a PSNR of 32.4 dB, SSIM of 0.92, and RMSE of 2.04, while NLM records lower values with a PSNR of 24.4 dB, SSIM of 0.73, and RMSE of 15.2. This trend continues across all MIAS images, demonstrating NLW's superiority over NLM. In the INbreast dataset, NLW maintains its lead. For instance, in Image 1, NLW shows a PSNR of 30.5 dB, SSIM of 0.93, and RMSE of 2.41, whereas NLM has comparatively lower scores with a PSNR of 19.2 dB, SSIM of 0.66, and RMSE of 12.5. Similar trends are observed in other INbreast images, indicating NLW's consistent denoising effectiveness. In DDSM, NLW continues to perform well. For instance, in Image 1, NLW achieves a PSNR of 31.9 dB, SSIM of 0.91, and RMSE of 4.81, while NLM records slightly lower values with a PSNR of 28.7 dB, SSIM of 0.79, and RMSE of 10.5. Across all DDSM images, NLW maintains a slight edge over NLM.

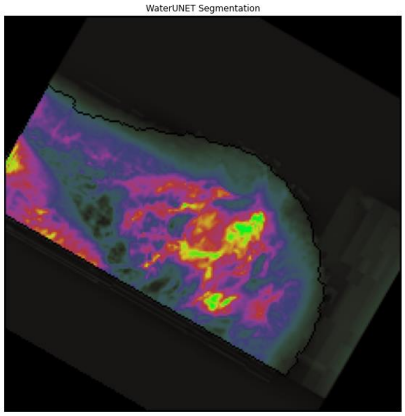


Figure 8: WaterUNet segmentation image

Figure 8 provides a visual representation of segmentation results obtained through the application of the WaterUNet model. Segmentation is a critical task in medical imaging, involving the delineation of specific regions or objects within an image.

**Table 3: Segmentation Accuracy comparison table**

| | | Segmentation Accuracy | | | | | |
|---|---|---|---|---|---|---|---|
| MIAS Dataset | Methods | Sobel | Prewitt | Watershed | CNN | UNET | WaterUnet |
| | Image 1 | 78 | 82 | 90 | 92 | 94 | 98 |
| | Image 2 | 88 | 81 | 91 | 93 | 95 | 97 |
| | Image 3 | 83 | 78 | 90 | 94 | 96 | 98 |
| | Image 4 | 86 | 80 | 88 | 92 | 94 | 99 |
| | Image 5 | 84 | 89 | 89 | 91 | 92 | 98 |
| INbreast | Image 1 | 81 | 85 | 89 | 95 | 96 | 99 |
| | Image 2 | 82 | 89 | 90 | 92 | 93 | 98 |
| | Image 3 | 87 | 81 | 90 | 91 | 92 | 94 |
| | Image 4 | 85 | 86 | 91 | 92 | 94 | 96 |
| | Image 5 | 79 | 83 | 88 | 94 | 95 | 97 |
| DDSM | Image 1 | 89 | 87 | 91 | 93 | 94 | 97 |
| | Image 2 | 88 | 88 | 91 | 90 | 94 | 98 |
| | Image 3 | 89 | 84 | 90 | 92 | 92 | 98 |
| | Image 4 | 82 | 89 | 91 | 97 | 97 | 99 |
| | Image 5 | 80 | 89 | 89 | 92 | 95 | 99 |

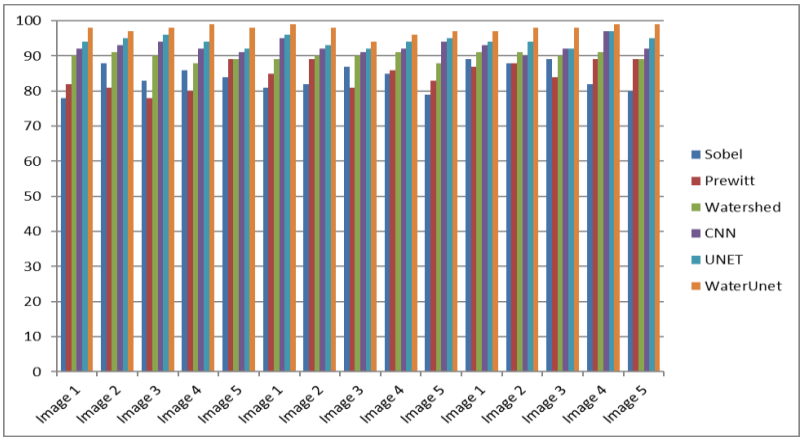


Figure 9: Segmentation accuracy comparison chart

The table 3 and figure 9 shows segmentation accuracy data performance of different segmentation methods (Sobel, Prewitt, Watershed, CNN, UNET, and WaterUnet) across three datasets: MIAS, INbreast, and DDSM, for various images. Across the MIAS dataset, WaterUnet consistently achieves the highest accuracy, reaching up to 99% accuracy in Image 4. UNET and CNN also perform well, consistently scoring above 90% accuracy. In the INbreast dataset, WaterUnet once again demonstrates superior performance, hitting 99% accuracy in multiple images, closely followed by UNET and CNN. For the DDSM dataset, WaterUnet outperforms other methods in almost all cases, achieving up to 99% accuracy in several images. This data emphasizes the effectiveness of advanced segmentation methods like UNET and WaterUnet, especially in medical imaging tasks, where precise segmentation is crucial for accurate diagnosis and analysis. These results suggest the potential of these techniques in improving the accuracy and reliability of medical image segmentation tasks.

**Table 4: Overall accuracy comparison table**

| | | CNN | DCNN | DNN | VGG19 |
|---|---|---|---|---|---|
| MIAS Dataset | Accuracy | 95 | 96 | 97 | 98 |
| | Precision | 94 | 95 | 96 | 97 |
| | Recall | 96 | 96 | 98 | 99 |
| | F-measure | 91 | 92 | 95 | 98 |
| INbreast | Accuracy | 96 | 97 | 97 | 98 |
| | Precision | 94 | 95 | 95 | 96 |
| | Recall | 95 | 94 | 96 | 99 |
| | F-measure | 91 | 92 | 94 | 97 |
| DDSM | Accuracy | 95 | 96 | 97 | 99 |
| | Precision | 94 | 95 | 95 | 97 |
| | Recall | 97 | 95 | 96 | 99 |
| | F-measure | 97 | 94 | 95 | 98 |

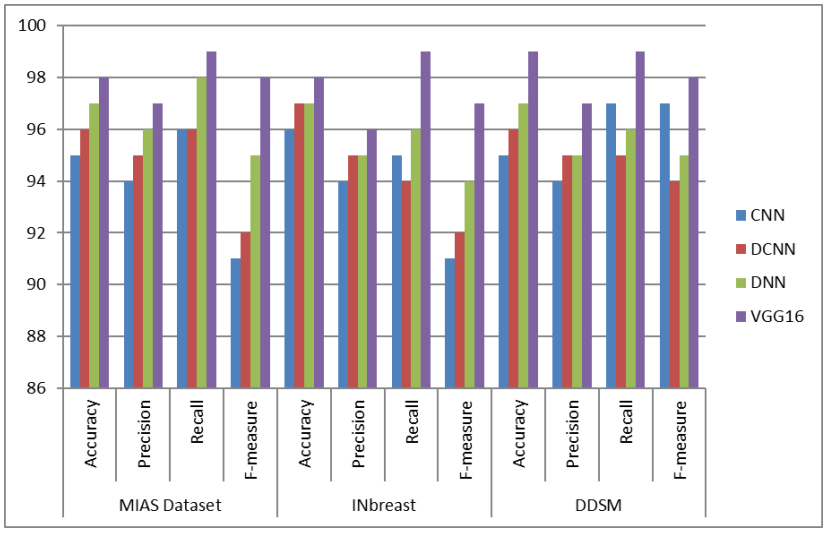


Figure 10: Overall accuracy comparison chart

The table 4 and figure 10 shows accuracy, precision, recall, and F-measure data across different models (CNN, DCNN, DNN, VGG19) on MIAS, INbreast, and DDSM datasets illustrates the comparative performance of these models in breast cancer classification. In the MIAS dataset, VGG19 demonstrates the highest accuracy (98%) and F-measure (98), indicating its robust ability to classify benign and malignant masses accurately. DCNN also performs well across all metrics, particularly in recall (98%) and precision (95%). Similarly, in INbreast, VGG19 and DCNN achieve remarkable results, with VGG19 leading in accuracy (98%) and F-measure (97). DCNN, on the other hand, excels in recall (96%) and precision (95%). For DDSM, VGG19 outshines other models with the highest accuracy (99%), recall (99%), and F-measure (98%). These results underline the effectiveness of deep learning models, especially VGG19, in accurately classifying breast masses. The high values across these metrics affirm the potential of these models in enhancing the reliability and precision of breast cancer classification, crucial for early detection and subsequent medical decisions.

## V. Conclusion

Finally, this study employs advanced image processing to detect breast cancer in a unique manner. We enhanced accuracy and efficiency by using a Hybrid Neural Network with VGG19 and modified DenseNet, improved Stochastic Gradient Descent (SGD), and cutting-edge denoising and segmentation methods. The hybrid neural network extracts detailed patterns from mammography images using VGG19 and a modified DenseNet, boosting the model's ability to detect malignant tissues. The enhanced SGD optimization approach ensures effective training, model convergence, and model longevity. The innovative Non-Local Means with Wavelet (NLW) Image Denoising method enhances mammography images. By reducing noise while keeping critical properties, NLW denoising offers high-quality images for trustworthy analysis, boosting breast cancer diagnosis. The most significant advance in this work is the use of WaterUNet for image segmentation. WaterUNet detects malignant spots in mammography. The accurate segmentation of WaterUNet enhances breast cancer diagnosis, allowing clinicians to make informed treatment decisions. In the MIAS dataset, VGG19 demonstrates the highest accuracy (98%) and F-measure (98), indicating its robust ability to classify benign and malignant masses accurately. DCNN also performs well across all metrics, particularly in recall (98%) and precision (95%). Similarly, in INbreast, VGG19 and DCNN achieve remarkable results, with VGG19 leading in accuracy (98%) and F-measure (97). DCNN, on the other hand, excels in recall (96%) and precision (95%). For DDSM, VGG19 outshines other models with the highest accuracy (99%), recall (99%), and F-measure (98%). Validating the proposed strategy on a diverse mammography dataset demonstrates that it outperforms current strategies. Because of the hybrid neural network, upgraded SGD algorithm, NLW denoising, and WaterUNet segmentation, it is a promising early breast cancer detection method.

## Reference

[1] A.Intasam et al., "Optimizing the Hyperparameter Tuning of YOLOv5 for Breast Cancer Detection," 2023 9th International Conference on Engineering, Applied Sciences, and Technology (ICEAST), Vientiane, Laos, 2023, pp. 184-187, doi: 10.1109/ICEAST58324.2023.10157611.

[2] A.Sinibaldi et al., "Direct Competitive Assay for ERBB2 Detection in Breast Cancer Cell Lysates Using 1-D Photonic Crystals-Based Biochips," in IEEE Sensors Letters, vol. 7, no. 8, pp. 1-4, Aug.

2023, Art no. 4501204, doi: 10.1109/LSENS.2023.3297372.

[3] D. Alsaedi, A. Melniko, K. Muzaffar, A. Mandelis and O. M. Ramahi, "A Microwave-Thermography-Convolution Neural Network Technique for Breast Cancer Detection," 2021 IEEE Asia-Pacific Conference on Applied Electromagnetics (APACE), Penang, Malaysia, 2021, pp. 1-2, doi: 10.1109/APACE53143.2021.9760519.

[4] D. Deepa, M. S. Raj, S. Gowthami, K. Hemalatha, C. Poongodi and P. Thangavel, "Identification and Analysis of Alzheimer's Disease using DenseNet Architecture with Minimum Path Length Between Input and Output Layers," 2022 Smart Technologies, Communication and Robotics (STCR), Sathyamangalam, India, 2022, pp. 1-5, doi: 10.1109/STCR55312.2022.10009552.

[5] D. Fajri Riesaputri, C. Atika Sari, I. M. S. De Rosal and E. Hari Rachmawanto, "Classification of Breast Cancer using PNN Classifier based on GLCM Feature Extraction and GMM Segmentation," 2020 International Seminar on Application for Technology of Information and Communication (iSemantic), Semarang, Indonesia, 2020, pp. 83-87, doi: 10.1109/iSemantic50169.2020.9234207.

[6] D. Kusumawati, A. A. Ilham, A. Achmad and I. Nurtanio, "Vgg-16 And Vgg-19 Architecture Models In Lie Detection Using Image Processing," 2022 6th International Conference on Information Technology, Information Systems and Electrical Engineering (ICITISEE), Yogyakarta, Indonesia, 2022, pp. 340-345, doi: 10.1109/ICITISEE57756.2022.10057748.

[7] G. Hamed, M. Marey, S. E. -S. Amin and M. F. Tolba, "A Proposed Model for Denoising Breast Mammogram Images," 2018 13th International Conference on Computer Engineering and Systems (ICCES), Cairo, Egypt, 2018, pp. 652-657, doi: 10.1109/ICCES.2018.8639307.

[8] G. Latif, M. O. Butt, F. Yousif Al Anezi and J. Alghazo, "Ultrasound Image Despeckling and detection of Breast Cancer using Deep CNN," 2020 RIVF International Conference on Computing and Communication Technologies (RIVF), Ho Chi Minh City, Vietnam, 2020, pp. 1-5, doi: 10.1109/RIVF48685.2020.9140767.

[9] H. M. Basha and G. Sindhu, "Improved Accuracy of Early Stage Breast Cancer Detection using Anisotropic Diffusion Algorithm And Variational Partial Differential Equation Method," 2022 International Conference on Sustainable Computing and Data Communication Systems (ICSCDS), Erode, India, 2022, pp. 1683-1689, doi: 10.1109/ICSCDS53736.2022.9760736.

[10] K. P. Adila and K. Sheeba, "Feature fused breast cancer detection," 2020 International Conference on Futuristic Technologies in Control Systems & Renewable Energy (ICFCR), Malappuram, India, 2020, pp. 1-5, doi: 10.1109/ICFCR50903.2020.9249995.

[11] M. Slimi, B. Jmai, P. Mendes and A. Gharsallah, "Breast cancer detection based on CPW antenna," 2019 IEEE 19th Mediterranean Microwave Symposium (MMS), Hammamet, Tunisia, 2019, pp. 1-4, doi: 10.1109/MMS48040.2019.9157301.

[12] M. U. Hoque, T. M. Shahriar Sazzad, A. K. M. A. Farabi, I. Hosen and M. A. Somi, "An Automated Approach to Detect Breast Cancer Tissue Using Ultrasound Images," 2019 1st International Conference on Advances in Science, Engineering and Robotics Technology (ICASERT), Dhaka, Bangladesh, 2019, pp. 1-4, doi: 10.1109/ICASERT.2019.8934546.

[13] M. Wang, J. Wu, D. Xu and S. Mao, "Optimization of Parallel Stochastic Gradient Descent on Sunway TaihuLight," 2020 2nd International Conference on Machine Learning, Big Data and Business Intelligence (MLBDBI), Taiyuan, China, 2020, pp. 18-23, doi: 10.1109/MLBDBI51377.2020.00010.

[14] N. Aziza and F. Samad, "Early Breast Cancer Detection with Microwave Imaging Technique by Using Spiral PIFA Antenna," 2021 5th International Conference on Electrical Information and Communication Technology (EICT), Khulna, Bangladesh, 2021, pp. 1-5, doi: 10.1109/EICT54103.2021.9733569.

[15] N. F. Razali, I. S. Isa, S. N. Sulaiman, N. K. A. Karim and M. K. Osman, "High-level Features in Deeper Deep Learning Layers for Breast Cancer Classification," 2021 11th IEEE International Conference on Control System, Computing and Engineering (ICCSCE), Penang, Malaysia, 2021, pp. 170-175, doi: 10.1109/ICCSCE52189.2021.9530911.

[16] P. E. Jebarani, N. Umadevi, H. Dang and M. Pomplun, "A Novel Hybrid K-Means and GMM Machine Learning Model for Breast Cancer Detection," in IEEE Access, vol. 9, pp. 146153-146162, 2021, doi: 10.1109/ACCESS.2021.3123425.

[17] P. K. Samanta, N. K. Rout and G. Panda, "A novel deep CNN model for improved breast cancer detection using ultrasound images," 2023 International Conference on Communication, Circuits, and Systems (IC3S), BHUBANESWAR, India, 2023, pp. 1-4, doi: 10.1109/IC3S57698.2023.10169383.

[18] S. Momtahen, M. Momtahen, R. Ramaseshan and F. Golnaraghi, "A Machine Learning Approach: NIR Scattering Data Analysis for Breast Cancer Detection and Classification," 2022 IEEE 1st Industrial Electronics Society Annual On-Line Conference (ONCON), kharagpur, India, 2022, pp. 1-6, doi: 10.1109/ONCON56984.2022.10127055.

[19] S. Zhang and L. Wang, "An improved non-local means filter for image mixed noise," 2021 China Automation Congress (CAC), Beijing, China, 2021, pp. 5545-5548, doi: 10.1109/CAC53003.2021.9727520.

[20] T. Gayathri, T. Madhavi and K. R. Kumari, "A Prediction of breast cancer based on Mayfly Optimized CNN," 2022 International Conference on Computing, Communication and Power Technology (IC3P), Visakhapatnam, India, 2022, pp. 176-180, doi: 10.1109/IC3P52835.2022.00044.

[21] U. Khasana, R. Sigit and H. Yuniarti, "Segmentation of Breast Using Ultrasound Image for Detection Breast Cancer," 2020 International Electronics Symposium (IES), Surabaya, Indonesia, 2020, pp. 584-587, doi: 10.1109/IES50839.2020.9231629.

[22] Y. Feng, X. Chen, L. Lilge, K. Zhang, B. Su and C. Lin, "Feasibility Analysis of Spectral Detection of Breast Cancer Based on Monte Carlo Method," 2022 IEEE International Conference on Manipulation, Manufacturing and Measurement on the Nanoscale (3M-NANO), Tianjin, China, 2022, pp. 368-372, doi: 10.1109/3M-NANO56083.2022.9941659.

[23] Z. Aizaz, K. Khare, A. Khursheed and A. Tirmizi, "Pix2Pix Generative adversarial Networks (GAN) for breast cancer detection," 2022 5th International Conference on Multimedia, Signal Processing and Communication Technologies (IMPACT), Aligarh, India, 2022, pp. 1-5, doi: 10.1109/IMPACT55510.2022.10029087.

[24] Z. KHOMSI, A. ELOUERGHI, A. AFYF and L. BELLARBI, "Contribution for the Early Detection of Breast Cancer by a Superficial Thermography Solution," 2020 International Conference on Electrical and Information Technologies (ICEIT), Rabat, Morocco, 2020, pp. 1-4, doi: 10.1109/ICEIT48248.2020.9113225.

[25] M. Robin, J. John and A. Ravikumar, "Breast Tumor Segmentation using U-NET," 2021 5th International Conference on Computing Methodologies and Communication (ICCMC), Erode, India, 2021, pp. 1164-1167, doi: 10.1109/ICCMC51019.2021.9418447.

M. SUBHA M.Sc., M.Phil., is pursuing Ph.D. in Computer Science (PT) in PG And Research Department of Computer Science in Erode Arts and Science College (Autonomous), Erode and working as an Assistant Professor and Head in the Department of Computer Science in Shree Venkateshwara Arts and Science (Co-Education) College, Gobichettipalayam from 2020 to till date. Her area of specialization is Data mining and Warehousing, Data Structures.

Dr.P. Srimanchari received B.Sc (Computer Scierence) degree from Erode Arts College for Women in 1995 and M.Sc Computer Science degree from Vivekanandha College of Arts and Science for Women in 2000. She obtained his M.Phil Degree in Computer Science from Erode Arts College in 2004. She did his Doctoral research from Bharathiar University, Coimbatore during 2010 – 2015. She is currently working as an Assistant Professor in Computer Science Department of Erode Arts and Science College, Erode Dr. P. Srimanchari research has spanned a large number of disciplines like Data Mining, Cloud Computing, Big Data Analysis and Wireless Sensor Networks. She has held positions as reviewer for different peer reviewed journals. As a member of various educational bodies in her career She has seventeen years of academic service alone she has been working closely with students, teachers, and colleagues. She is currently guiding four Ph.D's, She has published and presented research papers in reputed International Journals and Conference proceedings